Measurement of Particle Concentration in a Wurster Fluidized Bed by Electrical Capacitance Tomography Sensors

Ruihuan Ge
Institute of Engineering Thermophysics, Chinese Academy of Sciences, PO Box 2706, Beijing 100190, China

University of Chinese Academy of Sciences, Beijing 100190, China

Jiamin Ye and Haigang Wang
Institute of Engineering Thermophysics, Chinese Academy of Sciences, PO Box 2706, Beijing 100190, China

Wuqiang Yang
School of Electrical and Electronic Engineering, The University of Manchester, Manchester M13 9PL, U.K

DOI 10.1002/aic.14595
Published online August 25, 2014 in Wiley Online Library (wileyonlinelibrary.com)

It is essential to measure and monitor the particle flow characteristics in a Wurster fluidized bed to understand and optimize the coating processes. In this article, two electrical capacitance tomography (ECT) sensors are used to measure the particle concentration in different regions in a Wurster fluidized bed for the "cold" particle flows. One ECT sensor has a 12-4 internal-external electrodes and another has eight electrodes. The 12-4-electrode ECT sensor is used to measure the particle concentration in the annular fluidization region (outside of the Wurster tube) and the eight-electrode ECT sensor is used to measure the particle flow in the central region (inside the Wurster tube). The effect of particle type, particle moisture, fluidization velocity, and geometrical parameters on the Wurster fluidization process is studied based on the two ECT measurements. The radial particle concentration profiles in the annular fluidization and central flow regions with different operation parameters are given. Fast Fourier Transform analysis of the particle concentration in the Wurster tube is performed with different superficial air velocities. The optimum operating ranges of the Wurster fluidization process for different particles are given. In the end of the article, computational fluids dynamics simulation results are given and used to compare with the measurement results by ECT for a typical Wurster fluidized bed. © 2014 American Institute of Chemical Engineers *AIChE J*, 60: 4051–4064, 2014
Keywords: electrical capacitance tomography, internal-external electrode, particle concentration, Wurster fluidized bed

Introduction

Wurster fluidized beds[1] are widely used for coating, drying, and granulation in chemical, pharmaceutical, energy, and other industries for solids dose formulation. The main advantage of using Wurster fluidized beds is that they can provide an efficient heat and mass transfer and can mix and agglomerate excipients and active material ingredients to produce uniform blending of particles.[2] The gas-solids flow in a Wurster fluidized bed can be divided into four typical flow regions based on the particle movement pattern: (1) a fast transport coating region in the Wurster tube, (2) a drying region, (3) an annular fluidization region, and (4) a horizontal transport region. In a granulation and coating process, water or water-based binding solution is sprayed onto the particle surface to increase adhesion forces so that agglomerating excipients can be formed in the Wurster tube. A drying process is the inverse process of granulation and coating in the drying region. During the drying process, water is extracted and other solvents are removed from particles to provide a sufficient shelf life. During a granulation, coating or drying process, particle properties, including particle density, particle-size distribution, viscosity, and restriction coefficient, may change dramatically due to the change in moisture and agglomeration. All these parameters would affect the hydrodynamic behavior of a Wurster fluidized bed.[3,4]

Currently, the most important issue for granulation and coating in a Wurster fluidized bed is the coating quality. The undesired agglomeration with high moisture content and high temperature occurs when the particles adhere to each other to form larger entities.[5] These entities can easily stick onto the hot wall, which results in fault granulation and drying. The coating uniformity is also an important evaluation factor, as uniform coating can mask taste, separate coated particles from their environment (water, acid, oxygen, and other food ingredients), and save coating materials.[6] To ensure good coating quality, it is necessary to understand the particle flow behaviors in different regions of a Wurster fluidized bed and find the optimum operating range. In addition, it is necessary to understand the fluidized bed coating and granulation process with a Wurster tube for scaling up a

Correspondence concerning this article should be addressed to H. Wang at wanghaigang@iet.cn.

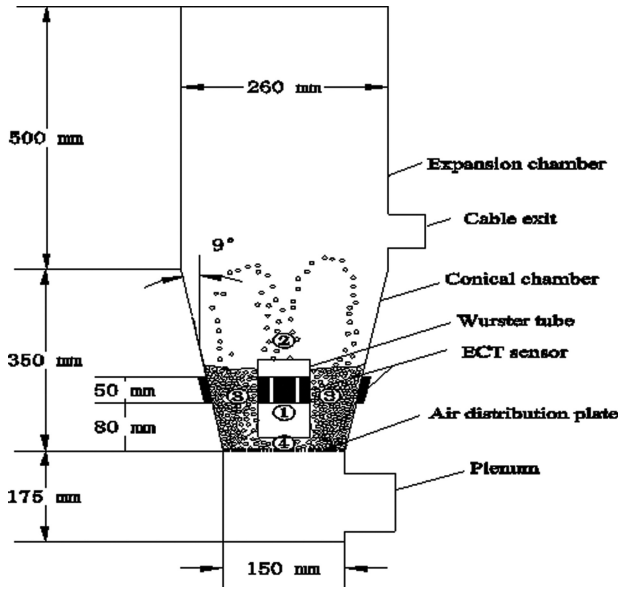

Figure 1. Wurster fluidized bed.

fluidized bed reactor from a small scale to a production scale.[7]

To understand and optimize the granulation and coating processes, it is essential to measure and monitor the particle concentration in a Wurster fluidized bed. In literature, some methods have been reported to measure the behavior of gas-particle two-phase flows in a Wurster fluidized bed or traditional spouted bed. He et al.[8] used a fiber optic probe to investigate the particle voidage profile in the fountain, spout and annulus of spouted beds. Saadevandi and Turton[9] applied computer-based video imaging techniques to measure particle velocity and voidage profile in a semicircular spouted-fluidized bed coating device. Karlsson et al.[10] developed a high-speed video camera technique to obtain particle trajectories in the fountain region of a Wurster fluidized bed. More recently, Luštrik et al.[11] designed a piezoelectric probe to estimate the impact rate of particles in the Wurster tube of a coating chamber. However, due to the complexity of the process, the measurement techniques used in these studies have many limitations and disadvantages. For instance, the fiber optic probe and piezoelectric probe are invasive measurement techniques and can only obtain local information and the video imaging technique can be only suitable for dilute flows.

Electrical capacitance tomography (ECT) is a mature technology for measuring gas-solids flow.[12,13] It is a nonintrusive noninvasive technique and can be utilized to measure the particle concentration and reconstruct the permittivity distribution in a cross section with a fast speed (>100 frames per second). Takei et al.[14] used ECT to visualize the particle movement in the draft tube of a spouted fluidized bed. However, the influence of different operation parameters was not investigated, and particle concentration distributions in the annular region were not obtained. Due to the Wurster tube in the fluidized bed, it is difficult to directly apply conventional ECT sensors and optical techniques to measure the particle concentration in the annular fluidization region.[15,16]

The objective of this research is to obtain the cross-sectional particle distributions in different regions of a Wurster fluidized bed, so that the particle behaviors can be understood and the optimum operating ranges can be found, based on ECT measurements. A new ECT sensor, which has twelve external electrodes and four internal electrodes, is designed to measure the particle concentration in the annular fluidization region. A traditional eight-electrode ECT sensor is used to measure the particle flow in the Wurster tube. The concentration profiles in these two regions are given based on ECT measurements. Fast Fourier transform (FFT) is introduced to analyze the time-series signal fluctuations of concentration in the Wurster tube. Different fluidization operation parameters, including particle type, particle moisture, fluidization velocity, and Wurster tube geometrical parameters are considered to investigate the particle flow behaviors of the fluidized bed. Computational fluids dynamics (CFD) simulation results are given to compare with the ECT measurement results for a typical Wurster fluidized bed process.

Experimental Setup

Test facility

A lab-scale Wurster fluidized bed is used in this research. The maximum capacity for each batch is 2.5 kg for coating. The fluidized bed chamber is made of Plexiglas consisting of a plenum, a conical part and an expansion part. The schematic diagram of the fluidized bed is illustrated in Figure 1. The diameter of the Wurster tube is 65 mm and the height is 150 mm. The thickness of the tube is 1.5 mm. The air distributor made of stainless steel with a diameter of 150 mm is a perforated disc and located beneath the Wurster tube. To control different flow regimes in the bottom of the chamber, the air distributor with different open area is introduced and designed as shown in Figure 2. The central region of the air distributor has large holes with an open area of 35%, which particles are accelerated upward through the Wurster tube with a suitable velocity. Surrounding the central region of the distributor is an annular area with smaller hoes containing 4% open area to allow air to flow into the annular fluidization region with a relatively low velocity to keep the particles with minimum fluidization condition in the annular

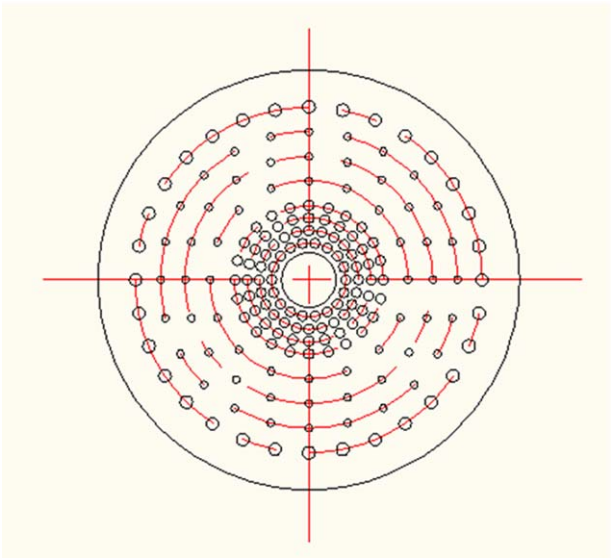

Figure 2. Air distributor.

[Color figure can be viewed in the online issue, which is available at wileyonlinelibrary.com.]

Table 1. Properties of Particles

	Material	Particle Density (kg/m^3)	Mean Particle Diameter (μm)	Packed Bed Concentration (%)
Particle I	Corn powder	1463	937	54
Particle II	Soghum rice	1441	2773	57

fluidization region. There exists complex interference between the annular and coating region for the gas-particles flow, especially near the bottom of the conical part, it is difficult to separate and quantify each flow rate precisely. The height of the gap between the Wurster tube and the air distributor can be adjusted from 5 to 15 mm.

Materials and experimental parameters

Two different types of particles have been used in this research, namely "Particle I" and "Particle II" as listed in Table 1. Tables 2 and 3 give the size distribution for Particle I and Particle II. The mean diameter of Particle I is 937 μm while Particle II has a mean diameter of 2773 μm. To minimize the electrostatic effects on ECT measurement, particles used in this study contain a moisture content of 5 wt % to reduce the static charge during particles interaction and increase the flow medium relative humidity.[17]

For Particle I, experiments were conducted with two different gap heights between the Wurster tube and the distributor (5 and 15 mm). The average superficial air velocities above the air distributor were varied from 0.94 to 2.83 m/s. For Particle II, the same gap heights were used, while the superficial air velocities were varied from 1.57 to 3.15 m/s correspondingly. The values of 0.94 and 1.57 m/s are chosen as the superficial velocity to start fluidization for each type of particles, respectively.

To investigate the influence of particle moisture, particles with different moisture content were prepared. A certain amount of distilled water was sprayed onto the dry particles and mixed in a low-speed food mixer for 10–20 min to ensure homogeneous moisture distribution. The wet particles were kept in an airproof environment with well-stabilized temperature and humidity and make sure agglomerations are removed. Samples were collected from each batch before and after each dynamic test. The moisture contents of these samples were measured by a moisture meter based on the loss on drying method as a reference.

ECT sensor design

Figure 3a shows the ECT sensor with 12-4 external-internal electrodes. In the following, the ECT sensor with internal-external electrodes is called "IEE sensor," which is used to measure the particle concentration in the annular fluidization region. The external electrodes are stuck to the outside wall of the conical chamber and the internal electrodes are mounted outside the Wurster tube, the external and internal screens are utilized to eliminate external interference. The external and internal electrodes are arranged at the same level above the air distributor. Each electrode has a length of 5 cm and the location of the sensor is depicted in Figure 1. The measurement region encompasses the height between 8 and 13 cm above the air distributor. The midposition of this region is 10.5 cm and each pixel in the ECT image represents an axial average over this cylindrical measurement volume.

Table 2. Particle Size Distribution of Particle I

Particle Size (μm)	Mass Percentage in Range (%)
>2000	0
1600–2000	9.47
1400–2000	1.48
1250–1400	15.38
950–1250	16.26
600–950	57.21
<600	0.18

Table 3. Particle Size Distribution of Particle II

Particle Size (μm)	Mass Percentage in Range (%)
>3200	0.01
2800–3200	70.44
2500–2800	13.64
2000–2500	12.85
1600–2000	2.70
<1600	0.35

Figure 3b shows the ECT sensor with eight electrodes. This sensor is applied to measure the particle concentration inside the Wurster tube. Electrodes are mounted inside the Wurster tube with screen stuck to the outside of the tube. The eight-electrode ECT sensor is installed at the same height of the Wurster tube with the IEE sensor. Figure 4 gives the integration of the 12-4 IEE and eight electrodes sensors. There are two insulating layers and one shielding layer between the two ECT sensors. The shielding layer is used to eliminate the electrostatic interference between the two sensors and reduce the cross-talking between the two measurements. An AC-based ECT system with 16 channels is used in the measurement. Due to the limitation in the channel number of the ECT system, the measurements are taken between the 12-4 IEE sensor and eight-electrode sensor separately in the Wurster fluidized bed process with the same operation conditions.

Figure 5 shows the picture of the Wurster fluidized bed with the constructed ECT sensors. As shown in Figure 5b, to reduce the cable effect on the flow hydrodynamics, the cables are connected to the internal electrodes of the tube passing through the upper part of the conical chamber separately. Due to the small cable diameter, the flow disturbances have been reduced to minimal both in the Wurster tube and annular fluidization region.

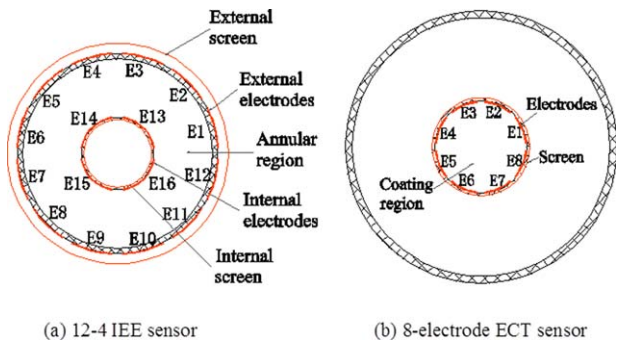

Figure 3. ECT sensor design.

[Color figure can be viewed in the online issue, which is available at wileyonlinelibrary.com.]

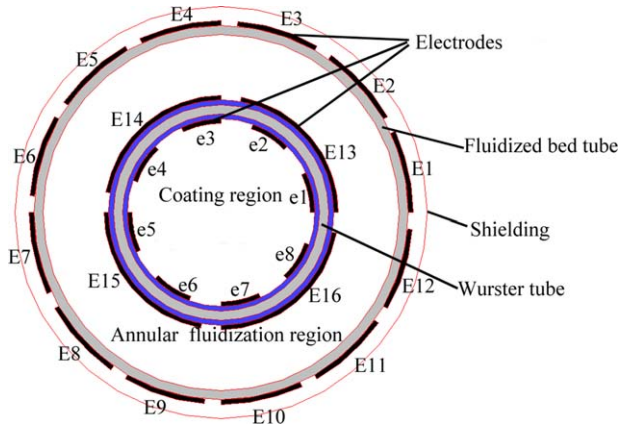

Figure 4. Integration of 12-4 IEE electrodes and eight-electrodes sensor.

[Color figure can be viewed in the online issue, which is available at wileyonlinelibrary.com.]

Sensitivity map

Figure 6 shows the typical potential distributions for the 12-4 IEE sensor, which is calculated using FEM software package Maxwell from Ansoft. Figure 7 shows typical sensitivity maps between different electrode pairs. There are totally 120 sensitivity maps for the 12-4 IEE sensor. These sensitivity maps will be used for image reconstruction. The potential distributions and sensitivity maps also indicate that there is no interference between the 12-4 IEE and eight-electrode sensors.

Measuring strategy

For a complete measurement procedure of the IEE sensor, the capacitances between all possible electrode pairs are measured, the total number of electrode combinations is

$$M=\frac{(N_{\mathrm{E}}+N_{\mathrm{I}})\cdot(N_{\mathrm{E}}+N_{\mathrm{I}}-1)}{2} \tag{1}$$

where N_{E} is the number of external electrodes and N_{I} is the number of internal electrodes. In this research, $N_{\mathrm{E}}=12$ and $N_{\mathrm{I}}=4$. The number of independent capacitance measurements is then 120.

For the eight-electrode ECT sensor, a dual-electrode excitation strategy is used, the total number of combinations of electrodes with dual-electrode excitation is

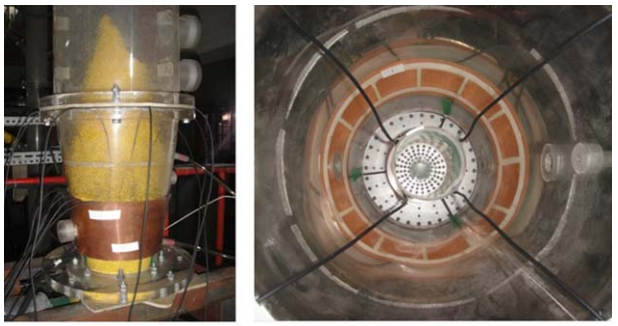

(a) Wurster fluidized bed (b) ECT sensor

Figure 5. Wurster fluidized bed with constructed ECT sensors.

[Color figure can be viewed in the online issue, which is available at wileyonlinelibrary.com.]

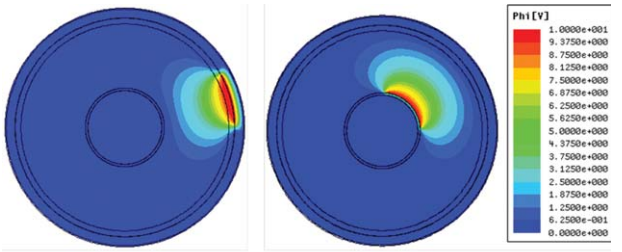

(a) Electrode 1 energised (b) Electrode 13 energised

Figure 6. Potential distribution of 12-4 IEE sensor.

[Color figure can be viewed in the online issue, which is available at wileyonlinelibrary.com.]

$$M=N\cdot(N-N_{\mathrm{EX}}) \tag{2}$$

where N is the number of electrodes and N_{EX} is the number of excitation electrodes. In this research, $N=8$ and $N_{\mathrm{EX}}=2$, the total number is 48.

Image reconstruction

The normalized capacitance vector λ is expressed as

$$\lambda=\frac{C_{\mathrm{M}}-C_{\mathrm{L}}}{C_{\mathrm{H}}-C_{\mathrm{L}}} \tag{3}$$

where C_{M} is the measured capacitance vector, C_{H} and C_{L} represent the capacitance vector measured in a packed bed and empty bed separately. In the calibration, C_{H} and C_{L} are first got before dynamic tests to normalize the measured capacitance C_{M}. The capacitance vector C_{H} in loose-packed bed change with varying particle moisture. To avoid the influence of particle moisture on the measurement, the ECT sensor was calibrated in different moisture content condition independently and saved as a datasheet. During the dynamic measurement of C_{M}, the C_{L} keeps fixed and C_{H} will be interpolated back into the saved datasheet based on the reference moisture content. More details on the influence of particle moisture and calibration methods are given in references.[18–20]

The normalized grey level vector G is calculated by

$$G=\frac{S^{T}\cdot\lambda}{S^{T}\cdot u_{\lambda}} \tag{4}$$

where S is the sensitivity matrix and u_{λ} is an identity vector.

To improve the image quality and measurement accuracy, a modified iteration method based on the Landweber algorithm is used for image reconstruction[20,21]

$$G^{\mathrm{n}+1}=G^{\mathrm{n}}\cdot(1.0+\tau)+\alpha\cdot S^{T}\cdot(\lambda-S\cdot G^{\mathrm{n}})\cdot(1-\tau) \tag{5}$$

where α is a step length or gain factor and τ is a relaxation factor.

The area-averaged particle concentration in a specific region of the whole cross section, β, is calculated by

$$\beta=\vartheta\cdot\bar{G}=\vartheta\cdot\frac{\sum_{i=1}^{K}G_i\cdot a_i}{\sum_{i=1}^{K}a_i} \tag{6}$$

where ϑ is the loose-packed bed concentration, which is 0.54 and 0.57, respectively, for the two types of particles, a is the area of each pixel, K is the effective pixel of the specific calculated region.

Before the dynamic tests, static tests were done to verify the reliability of ECT measurements. Figure 8 shows the

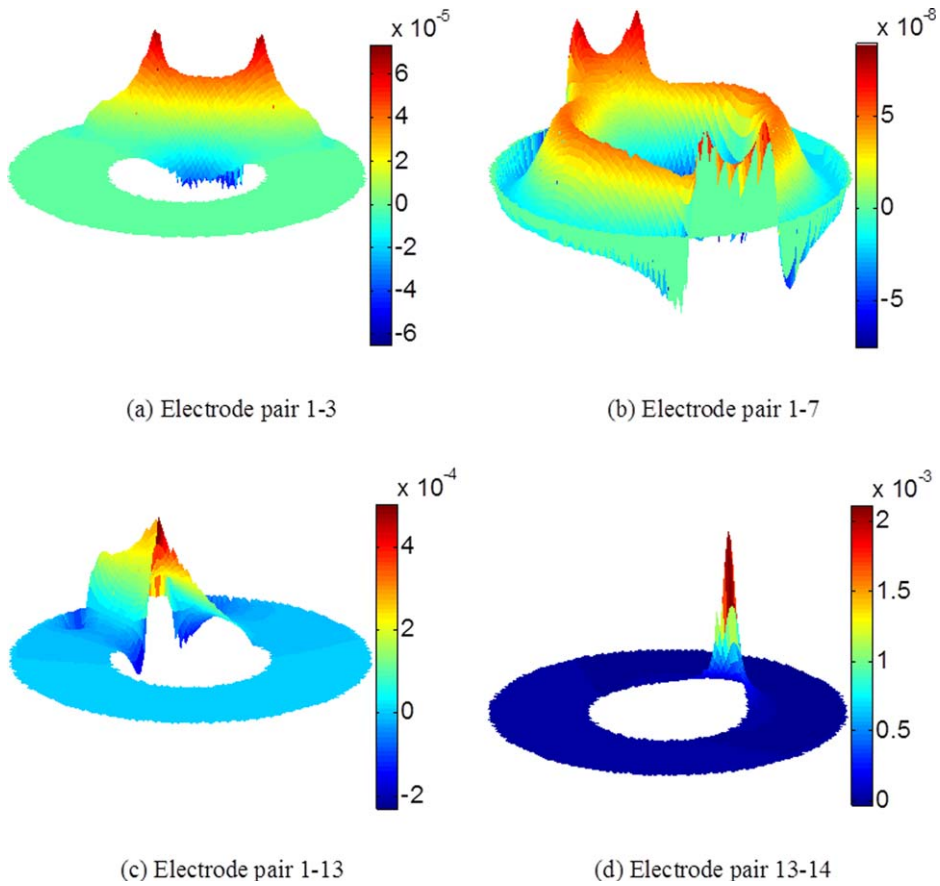

Figure 7. Typical sensitivity maps of 12-4 IEE sensor.

[Color figure can be viewed in the online issue, which is available at wileyonlinelibrary.com.]

radial particle concentration for a loose-packed bed calculated by Eqs. 3–6. The annular region is divided into 13 portions along the radial direction while the Wurster tube region is divided into 17 portions. It can be found that for all experimental conditions, ECT measurements give good agreement with the concentration in real loose-packed bed condition. More details on static measurement and calibration for the 12-4 IEE sensor have been given in references.[22,23]

In the dynamic tests, 2000 frames data were collected from the IEE sensor while 6000 frames data collected at 100 Hz from the eight-electrode ECT sensor. To ensure the repeatability, the measurements are consecutively repeated three times with the same experimental conditions.

Results and Discussion

Image reconstruction for particle concentration

Particle Concentration in Annular Fluidization Region. According to Eq. 6, the average particle concentration along the radial direction of annular fluidization region can be calculated and is shown in Figure 9. It can be seen from Figure 9 that the particle concentration profile changes with different type of particles and the height of gap. For Particle I with a gap of 5 mm, particles move downward smoothly in the annular region, the particle concentration nearly equals to the loose-packed concentration except for the condition of 2.83 m/s where bubbles begin to appear. In the case of 15 mm gap, the loosely packed bed can only be found at

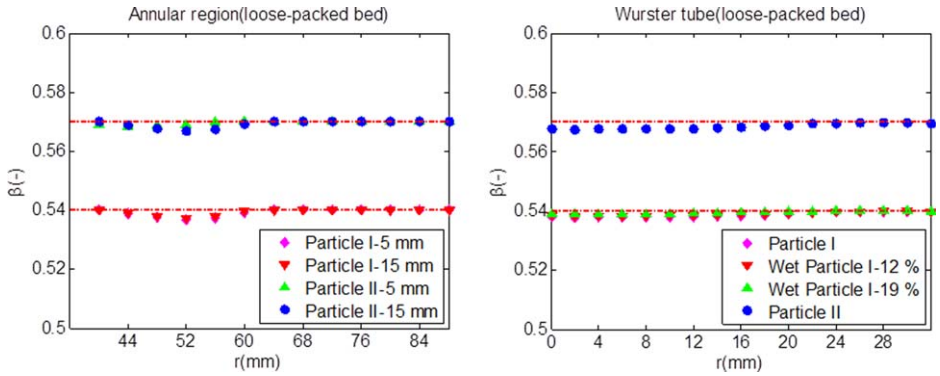

Figure 8. Radial profiles of packed bed concentration.

[Color figure can be viewed in the online issue, which is available at wileyonlinelibrary.com.]

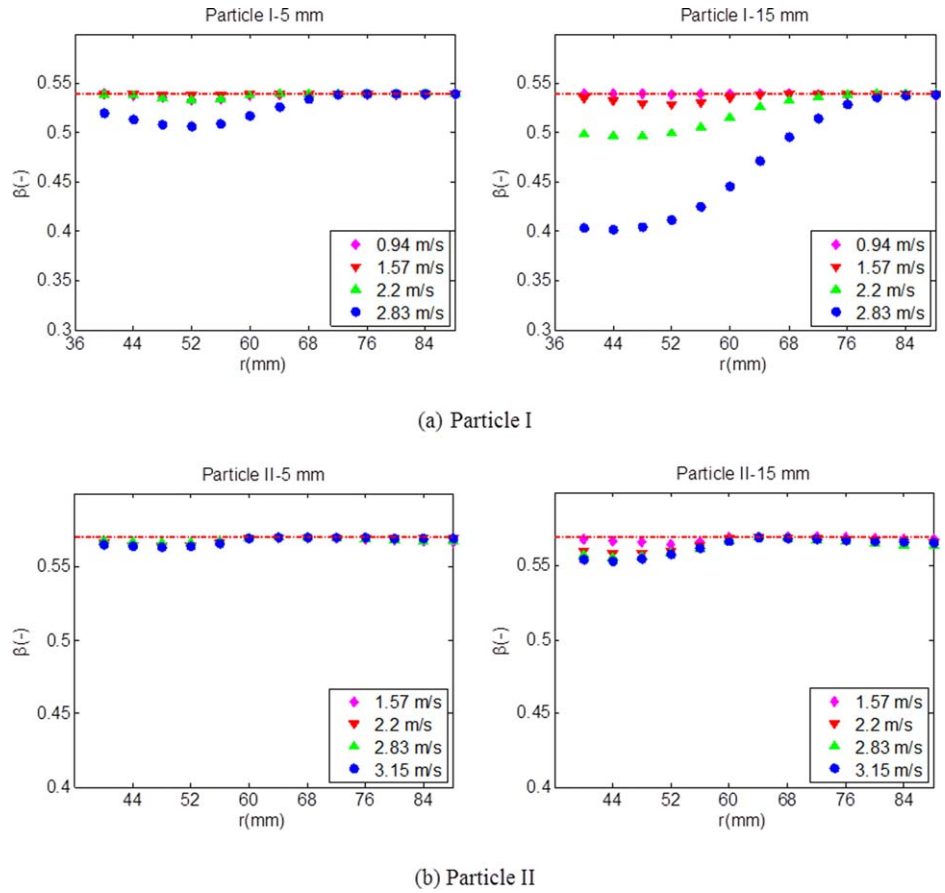

Figure 9. Radial profiles of particle concentration with different air velocity and gap in annular fluidization region.

[Color figure can be viewed in the online issue, which is available at wileyonlinelibrary.com.]

0.94 m/s. After that, the flow pattern is transformed into a bubbling bed and intense fluctuation can be observed when the air velocity is increased to 2.83 m/s. Figure 10 gives typical images of bubbles with different experiment conditions for Particle I. It can be found that the bubbles appear at a lower air velocity with the increased gap, and the bubble diameter increases with the increase in air velocity. In a real coating process, air bubbles can be harmful to the coating quality, the optimum operating conditions should be kept away from this flow regime and effective measures such as placing lamellas around the Wurster tube can be taken to reduce bubbles.[24,25]

For Particle II, bubbling behaviors are not found in all experimental cases in the annular fluidization region, and the concentration nearly equals to a loose-packed bed as shown in Figure 9b. For a gap of 15 mm, the concentration of the particles close to the Wurster tube wall decreases slightly when the air velocity is greater than 2.2 m/s. There are several reasons for this phenomenon. First, it can be observed that the bed height decreased from the conical chamber wall to the Wurster tube in the radial direction and even lower than the location of internal electrodes, this will affect the reconstructed images and measurement results. Second, the air flow is increased with the increase in the height of gap and the intensive of flow mixing between the coating and annular region becomes stronger and resulting in a higher voidage in the annular fluidization region.

Particle Concentration in Wurster Tube Region. Figure 11 shows the radial concentration profile of Particle I for different experimental setups in the Wurster tube. For both heights of gap, the particle concentration decreases from the wall to the center of the tube at 0.94 m/s, which represent the typical particle distribution at the initial fluidization velocity. With the increase in air velocity, a different height of gap presents a different radial profile.

For a gap of 5 mm, the concentration presents controversy trends compared with those obtained at 0.94 m/s. Specifically, the concentration in the center is higher than those near the tube wall. The profiles from the experimental and simulation results are quite similar to each other for a spouted bed with a draft tube.[9,26] The change in concentration profile indicates that particle flow is transited into another flow regime. By visual observation, the trajectory of particles in the tube becomes more regularly and the heights of the fountain of drying region become higher and higher with the increase in air velocity in this flow regime. The transition can also be found from the reconstructed images as shown in Figure 12.

For a gap of 15 mm, the particles distribution along the radial direction becomes irregular when the air velocity is larger than 0.94 m/s. Moreover, regular particle trajectories in the coating and drying region can hardly been observed in this operating range, that is, the particles are scattered across the whole cross section as depicted in Figure 12.

Average cross-sectional particle concentrations at different air velocities are given in Figure 13. It can be seen that the concentration drops sharply at 1.57 m/s with a gap of 5 mm. It corresponds to the flow regime transition. After that, the concentration nearly keeps stable in the range between 0.08 and

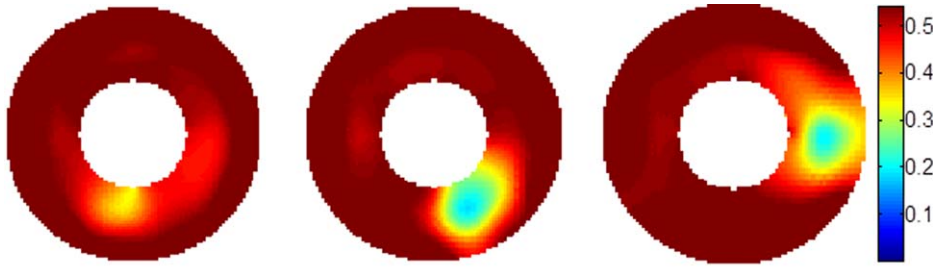

(a) Gap height = 5 mm, Air velocity = 2.83 m/s

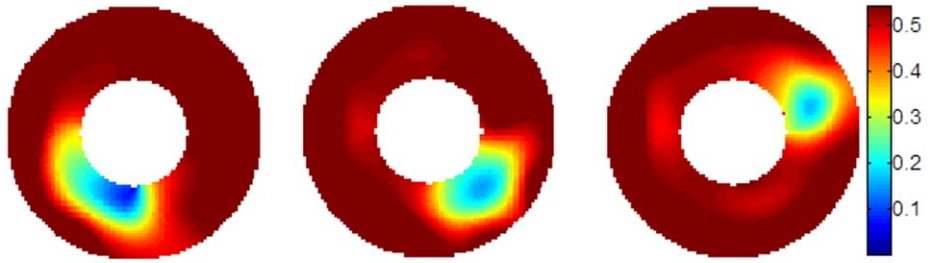

(b) Gap height = 15 mm, Air velocity = 2.2 m/s

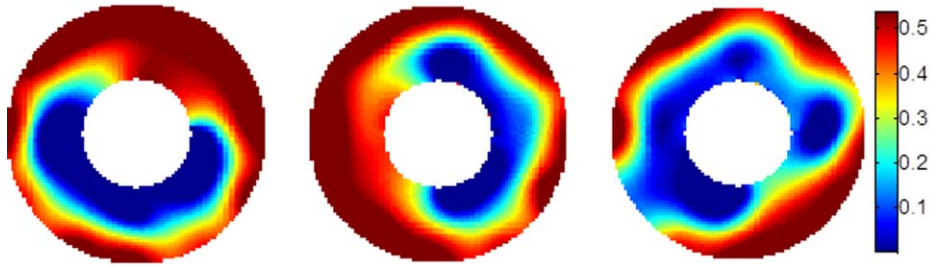

(c) Gap height = 15 mm, Air velocity = 2.83 m/s

Figure 10. Typical bubbling behavior in different experiments of Particle I.

[Color figure can be viewed in the online issue, which is available at wileyonlinelibrary.com.]

0.09. However, the turning point cannot be found at the gap of 15 mm. More specifically, the particle concentration drops linearly from 0.23 to 0.11 with the increase in air velocity.

Figures 14 and 15 show the radial profiles of concentration and typical reconstructed images of Particle II. At 1.57 m/s, the particle concentration decreases from the wall to the center of the tube, which represents the start of fluidization in the Wurster tube. When the air velocity is larger than 1.57 m/s, particles have a high concentration in the center of the Wurster tube.

Figure 16 shows the average cross-sectional particle concentration in the Wurster tube. At a gap of 5 mm, a turning

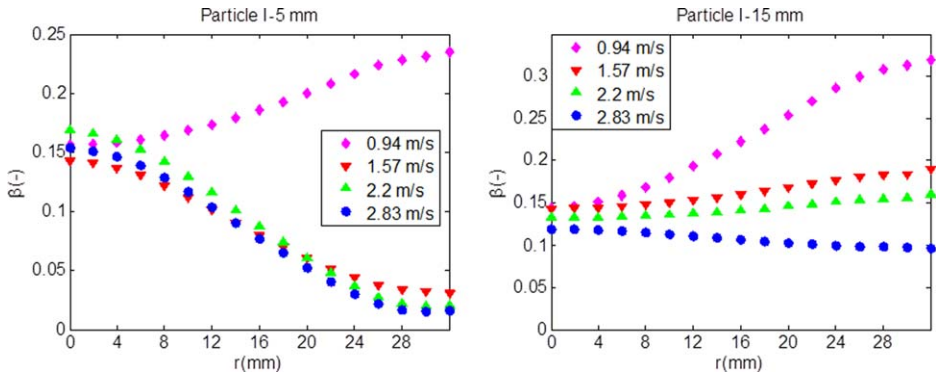

Figure 11. Concentration profile of Particle I with different air velocity and gap in Wurster tube.

[Color figure can be viewed in the online issue, which is available at wileyonlinelibrary.com.]

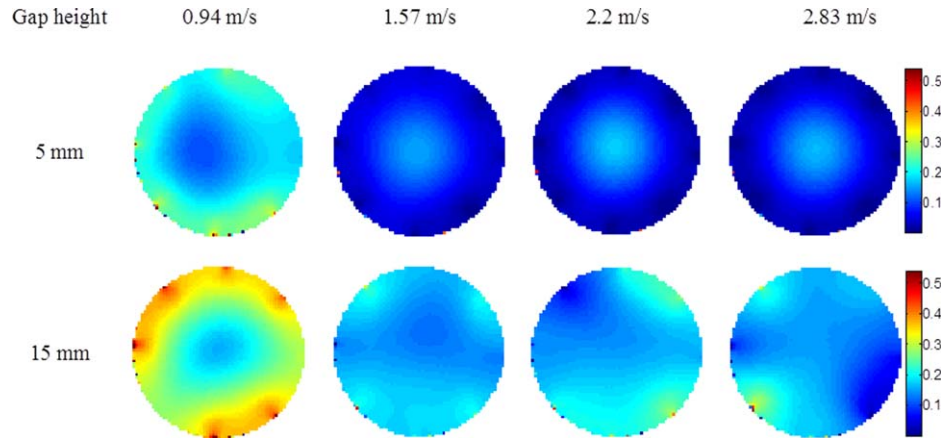

Figure 12. Typical images of Particle I in Wurster tube.

[Color figure can be viewed in the online issue, which is available at wileyonlinelibrary.com.]

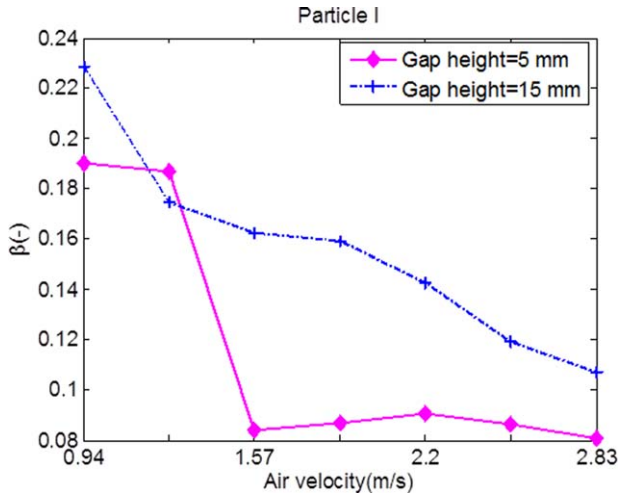

Figure 13. Average particle concentration of Particle I vs. air velocity in Wurster tube.

[Color figure can be viewed in the online issue, which is available at wileyonlinelibrary.com.]

point can be found at 2.83 m/s. Before the turning point, the particle concentration varies from 0.18 to 0.21, which indicates that too many particles are inhaled from outside of the Wurster tube, and regular particle flows cannot be formed due to mutual shadowing of particles.[24,27] After 2.83 m/s, the particle concentration decreases and stabilizes at 0.09, and particles are transported uniformly in the Wurster tube. At a gap of 15 mm, the turning point of concentration change occurs at 2.2 m/s. From this point onward, the concentration becomes stable. It can be concluded that particle trajectories in the Wurster tube tend to be more regular with the increase in air velocity after a turning point. In the meantime, particle concentrations are less sensitive to the air velocity, providing a wide range of process operation in a Wurster fluidized bed.

Analysis of particle concentration fluctuations in Wurster tube

In a coating process with a Wurster fluidized bed, uniformity of the end-point product is an important parameter to evaluate the coating quality.[28] The coating uniformity depends mainly on the coating-per-pass distribution and the cycle time that influenced by the operating parameters, such as the air velocity and the height of gap.[29] Therefore, it is meaningful to investigate the gas-particle flow behavior in the time and frequency domains in the Wurster tube to improve the circulation of particles and ensure coating uniformity. To have a deep understand of the particle fluctuations, FFT is applied.

Figure 17 shows the fluctuation of Particle I in terms of concentration and the corresponding power spectrum patterns. The characteristic frequency band is around 0 to 10 Hz with the superficial air velocity of 0.94 m/s. At this velocity, particles start to move upward in the center of the Wurster tube and particles fluctuate dramatically, which can

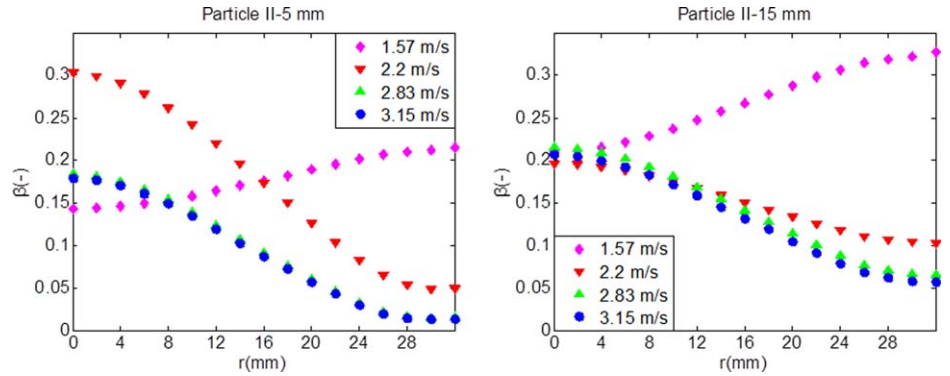

Figure 14. Concentration profiles of Particle II with different air velocity and gap in Wurster tube.

[Color figure can be viewed in the online issue, which is available at wileyonlinelibrary.com.]

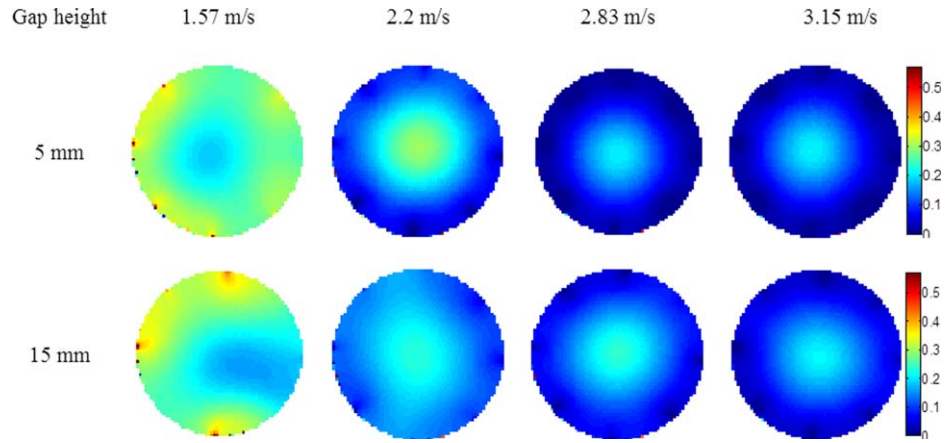

Figure 15. Typical images of Particle II in Wurster tube.

[Color figure can be viewed in the online issue, which is available at wileyonlinelibrary.com.]

be seen clearly in Figure 17a. It can be found that the characteristic frequency band moves toward a higher frequency region with a lower magnitude when the velocity is increased to 1.57 and 2.2 m/s. The fluctuation of particle becomes mildly with the increase in air velocity and levels off at 2.2 m/s. These two cases correspond to the optimal states of the Wurster process. When the air velocity is increased to 2.83 m/s, a characteristic frequency band becomes 1 to 4 Hz, and particles fluctuate dramatically again in the Wurster tube. In this case, a large amount of air passes through the annular fluidization region, and bubbling behavior appear as shown in Figure 10a. The bubbles have negative effect on the circulation of particles and hence the bubbling flow regime should be avoided in a Wurster fluidized bed coating process.[11]

For Particle II as shown in Figure 18, the particles have strong fluctuation in the Wurster tube at the air velocity of 1.57 m/s. The main frequency is around 0 to 10 Hz, which represents a typical characteristic spectral band of the initial fluidization state. With further increase in the air velocity, the movement of particles becomes stable and the characteristic frequency band changes to the region of 5–35 Hz while the power spectrum magnitude is considerably low. It can be inferred from the results that the particle circulation rate can be improved by increasing the air velocity for Particle II with a gap of 15 mm. The power spectrum is different from those of Particle I as the bubbling behavior cannot be found in all experiments for Particle II. The FFT results indicate that the fluctuation in the Wurster tube varies with different particles, with the increase in the superficial air velocity.

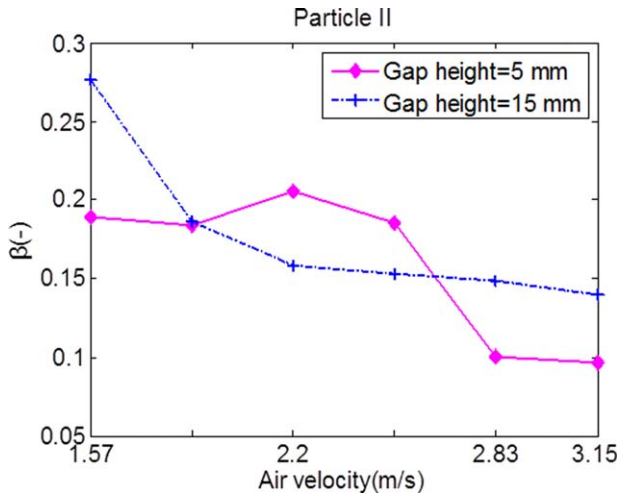

Figure 16. Average particle concentration of Particle II vs. air velocity in Wurster tube.

[Color figure can be viewed in the online issue, which is available at wileyonlinelibrary.com.]

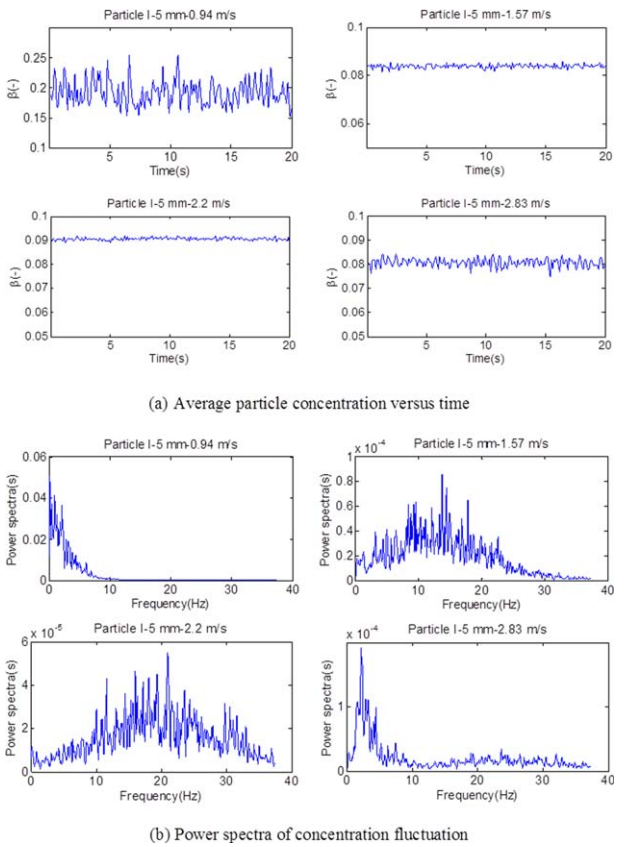

Figure 17. Particle concentration fluctuation and corresponding power spectra of Particle I.

[Color figure can be viewed in the online issue, which is available at wileyonlinelibrary.com.]

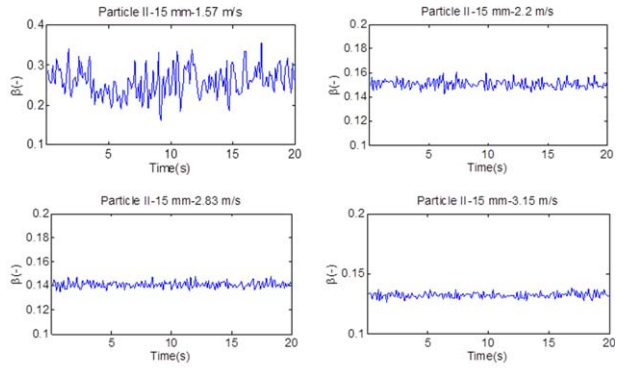

(a) Average particle concentration versus time

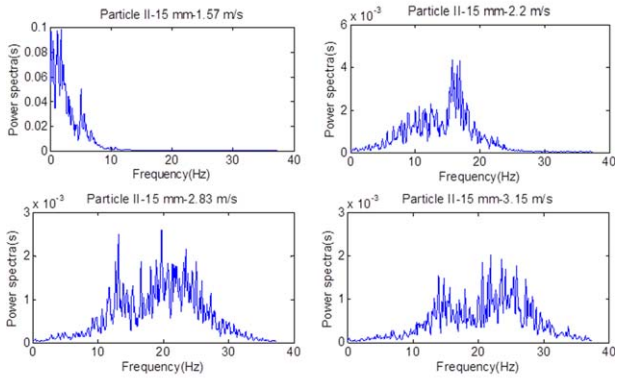

(b) Power spectra of concentration fluctuations

Figure 18. Particle concentration fluctuation and corresponding power spectra of Particle II.

[Color figure can be viewed in the online issue, which is available at wileyonlinelibrary.com.]

Optimum operating conditions for a Wurster fluidized bed

As discussed in Frequency domain analysis on particle concentration by FFT, the optimum flow state is characterized by the high frequency spectral band and low amplitude. For an optimum state, the characteristic spectral band is around 5–35 Hz with a low power spectrum magnitude (lower than 0.01). In this flow state, the fluctuations of particle become mildly and the average cross-sectional particle concentrations are less sensitive to the change in the air velocity as discussed before. This can lead to a better coating-per-pass distribution and cycle time distribution which is helpful to the end-point coating quality.[28] By contrast, in the start fluidization or bubbling state, the main frequency is less than 10 Hz with high magnitude. The fluidization is unstable and particles are transported in an irregular way in the central region. To find out the optimum operating range for different particles, the main frequency and corresponding amplitude of different experimental setups are given in Figure 19.

For Particle I, a wide operating range can be found between 1.57 and 2.6 m/s with a gap of 5 mm and the reuslt is shown in Figure 19a. With a lower velocity, particles move irregularly in the Wurster tube and a higher velocity results in a bubbling bed in the annular region. The optimum state can only be found at 1.57 m/s when the Wurster tube was moved vertically to the 15 mm gap. With the furture increase in the air velocity, bubbles appear in the annular region, which should be avoided in a Wurter fluidized bed coating process.[11]

For Particle II, a wide operating range can be found when the air velocity is larger than 2.2 m/s with a gap of 15 mm as shown in Figure 19b. As for the 5 mm gap height case, the opearating state can only be found when the air velocity is larger than 2.83 m/s. The bed keeps fixed before the point of 2.83 m/s.

Influence of particle moisture

In a real coating process, coating spray into the Wurster tube will result in the change in moisture in the process. The flow hydrodynamics may change due to different particle moisture.[19] To investigate the effect of moisture on the particle flow behavior in the Wurster tube, comparative tests were carried out with different particle moisture contents (11.68 and 18.43 wt %). Figure 20 shows the average particle concentration in a cross section for Particle I in the Wurster tube. It can be found that the effect of moisture on the particle concentration can be neglected with different air velocity. Figure 21 shows a typical power spectrum distribution for wet particles in the Wurster tube. At the minimum fluidization state (0.94 m/s), the characteristic frequency bands are around 0–10 Hz for different particle moisture. When the air velocity is increased to 2.2 m/s, which is the optimum state as discussed before, the characteristic frequency bands of these two experimental setups are all concentrated in the region between 5 and 35 Hz. The characteristic frequency bands and corresponding amplitudes are nearly the same as dry particles as shown in Figure 17b. The results indicate that the effect of increased moisture (up to 18.43 wt %) on the particles flow can be neglected in the Wurster tube. However, the moisture effect on the particle flowability is complex and it depends on the amount of water and the particle pore structure.[30] Further research need to be addressed to investigate the moisture effect on the particle flow using different type of powder and further increasing the moisture content.

CFD Simulation Results

CFD simulation was carried out to compare with the ECT measurements in the Wurster fluidized bed for Particle I. The control-volume-based code FLUENT 6.2 was chosen. The particle properties are the same as the ECT measurement and the particle diameter was supposed to be uniform distribution with a mean diameter of 937 μm, same as used in the ECT test. The time step was set to 5×10^{-4}s, to make sure the convergence. The CFD model used is based on the two-fluid model, which in turn, is based on the kinetic theory for granular flows.[31] A detailed discussion of the numerical method was given earlier by the authors.[31,32] The initial and boundary conditions for the CFD simulation are given in Table 4.

Instantaneous velocity and particle concentration distribution

Figure 22 shows the computed instantaneous particle and gas phase velocity in the *x-z* sliced plane. Figure 23 shows the instantaneous particle concentration in the *x-z* and *x-y* sliced planes for Particle I with a superficial air velocity of 0.94 m/s. The particle velocity shown in Figure 22a clearly demonstrates the motion of Particle In the annular fluidization region and fast transport coating region in the center of

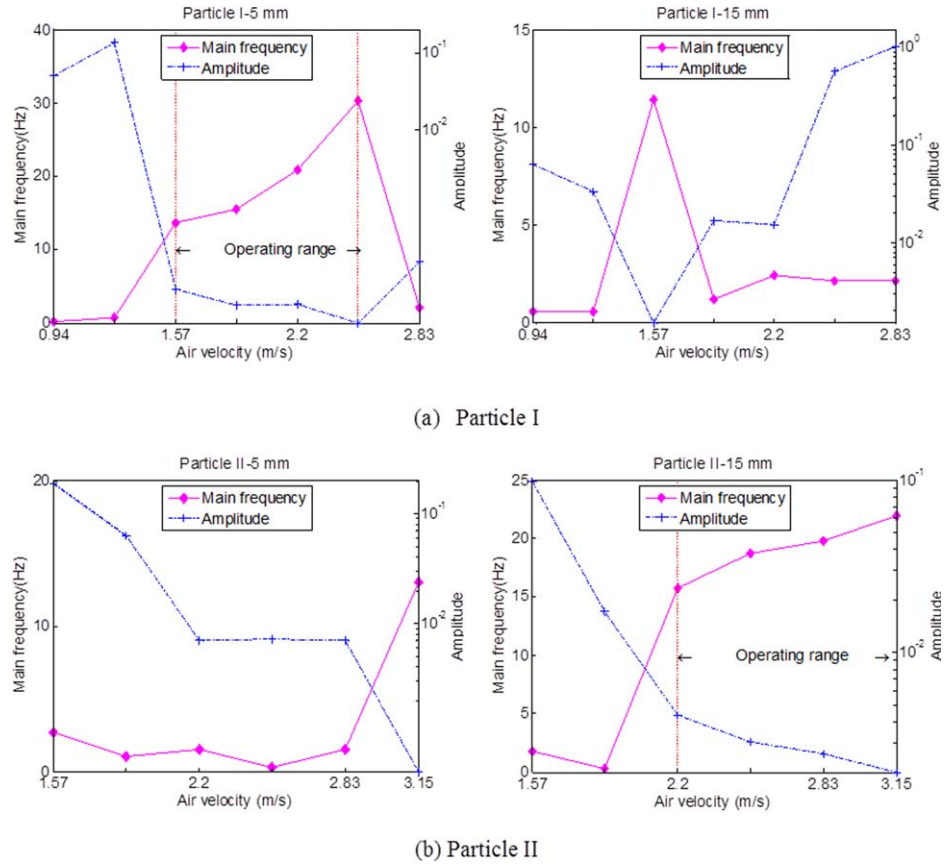

Figure 19. Main frequency and corresponding amplitude of different experimental setups.

[Color figure can be viewed in the online issue, which is available at wileyonlinelibrary.com.]

Wurster tube. The particle velocity clearly shows that most particles move downward in the top of the annular fluidization region and move upward in the Wurster tube. Comparing the CFD simulation results with ECT measurements as shown in Figures 10 and 12 for Particle I, the particle concentration in the *x-y* cross-section has nearly the same distribution, that is, bubbles in the annular fluidization region and core-annular distribution in the Wurster tube. The CFD simulation results agree well with the ECT measurements.

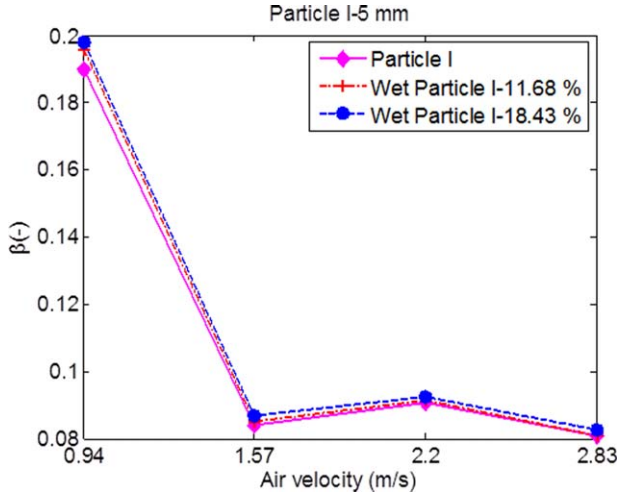

Figure 20. Comparison of average particle concentration in Wurster tube in terms of particle moisture.

[Color figure can be viewed in the online issue, which is available at wileyonlinelibrary.com.]

Time-average particle concentration profile

Figure 24 shows the time-averaged particle concentration from both CFD simulation and ECT measurements for Particle I with a superficial gas velocity of 0.94 m/s. CFD simulation gives the average particle concentration at four different positions above the air distributor, namely $z = 10.5$, 12.5, 14.5, and 16.5 cm, respectively, while ECT gives the average value at the position $z = 10.5$ cm above the air distributor. The CFD results agree well with the ECT measurements in the central region. However, in the near wall region, there is a discrepancy between CFD simulation and ECT measurement results. The main reasons can be summarized as follow. The CFD model used in this research only includes one single particle diameter distribution and the parameter used for the viscosity coefficient for solids phase is from a semiempirical function. However, there is particle diameter distribution in the real ECT measurement, which would result in slightly different hydrodynamic behavior in the fluidized bed.

Conclusions

In this article, ECT sensors are used to measure the particle concentration for a Wurster fluidized bed. A new ECT sensor with internal-external electrodes is designed to measure the particle concentration in the annular fluidization region, and a traditional eight-electrode ECT sensor is used to measure the particle concentration in the Wurster tube.

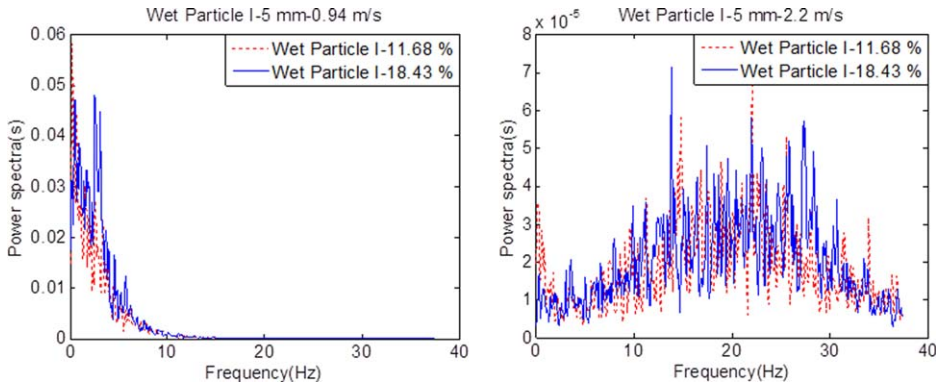

Figure 21. Comparison of power spectra in Wurster tube in terms of particle moisture.

[Color figure can be viewed in the online issue, which is available at wileyonlinelibrary.com.]

Table 4. CFD Model Parameters and Boundary Conditions

Parameter	Value	Comment or Reference
Particle diameter (d_s)	0.937 mm	No size distribution
Particle density (ρ_s)	1463 kg/m^3	–
Coefficient of restitution (e) (Particle–Particle Interaction)	0.9	Pain et al.[32]
Coefficient of restitution (e) (Particle-wall interaction)	0.75	Pain et al.[32]
Time step (Δt)	5 e−4 s	For convergence
Settled bed height (h)	200 mm	Fixed value

In the annular fluidization region, the particle distribution varies with different particles. Bubbles can easily be formed for Particle I in the annular region, which have a negative impact on the coating process. In the Wurster tube, radial concentration profiles are different in terms of different operating parameters. For most cases, the average particle concentration in a cross-section and air velocity curve has a turning point, which indicates the transition of flow pattern in the Wurster tube.

From the perspective of particle concentration fluctuation in time and frequency domains, the FFT analysis results show that the characteristic of fluctuation changes in the Wurster tube with particle type, fluidization velocity and gap height. The optimum operating ranges for different particles are given based on the FFT analysis. For Particle I, the operating range is between 1.57 and 2.6 m/s at 5 mm gap. For Particle II, the operating range can be found when the air velocity is larger than 2.2 m/s at a gap of 15 mm.

The comparative tests reveal that the effect of increased moisture (up to 18.43 wt %) on the particles motion can be neglected in the Wurster tube for the ECT measurement. The computed instantaneous velocity and particle concentration distribution show that the simulation results agree well with the ECT measurements.

The above results demonstrate that the proposed ECT sensors can be used to measure the particle concentration in the lab-scale Wurster-type fluidized bed. The ECT sensors provide cross-sectional information both in the annulus and Wurster tube regions. It provides a possibility to monitor and

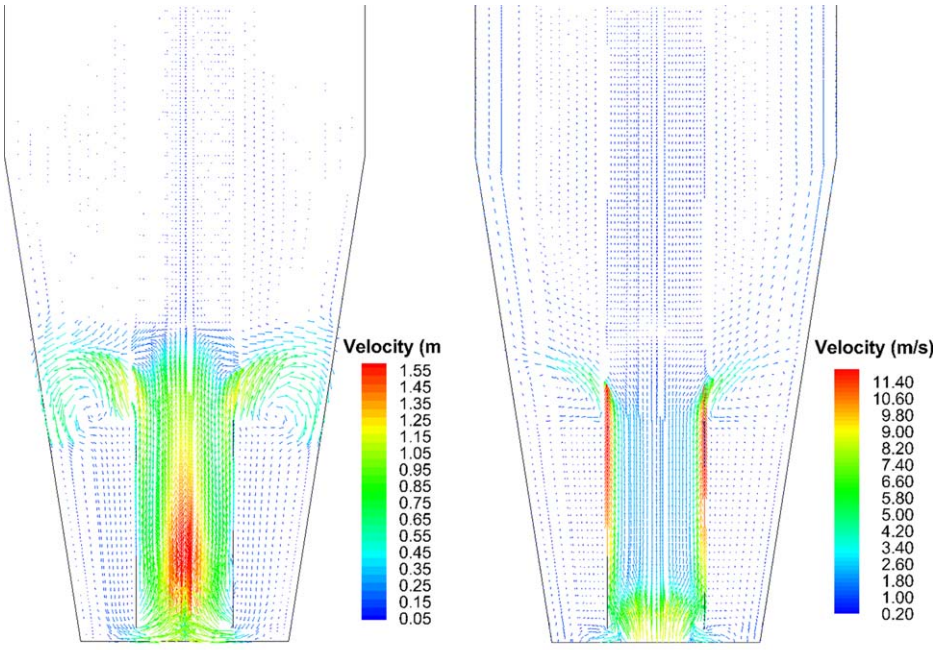

(a) Particle velocity (b) Gas phase velocity

Figure 22. Velocity vector distribution.

[Color figure can be viewed in the online issue, which is available at wileyonlinelibrary.com.]

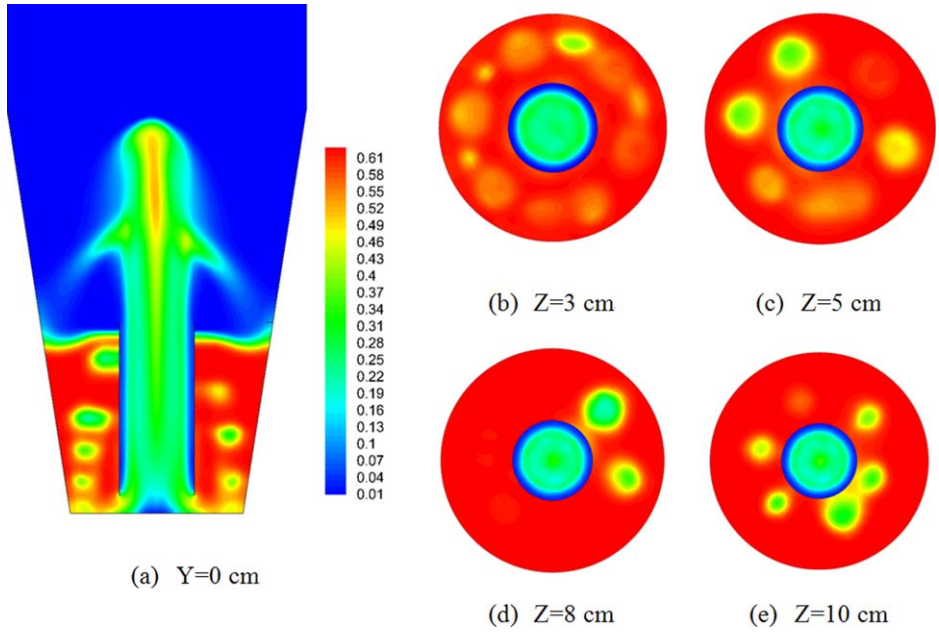

Figure 23. Particle concentration from CFD simulation.

[Color figure can be viewed in the online issue, which is available at wileyonlinelibrary.com.]

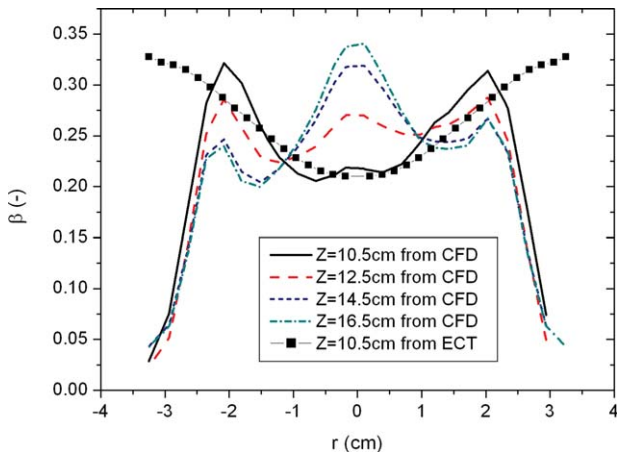

Figure 24. Comparison of particle concentration profiles by CFD and ECT for Particle I.

[Color figure can be viewed in the online issue, which is available at wileyonlinelibrary.com.]

optimize the coating process of a Wurster fluidized bed. Future work is needed to optimize the design of electrodes to improve measurement in terms of image error. Furthermore, efficient electrode construction and cable layout design are keys to the success of this technology applied to the fluidized beds coating in industry.

Acknowledgment

The authors would like to thank the National Natural Sciences Foundation of China (No. 61320106004) and Chinese Academy of Sciences "Hundred Talent Project" for financially supporting this research.

Notation

N = total number of electrodes
N_E = number of external electrodes
N_I = number of internal electrodes
N_{EX} = number of excitation electrodes
M = number of electrodes' combinations
C_H = capacitance vector in loose-packed bed, pF
C_L = capacitance vector in empty bed, pF
C_M = measurement capacitance vector, pF
S = sensitivity matrix
G = normalized grey level vector
G^n = G obtained in n-th iteration
u_λ = identity vector
a = area of each pixel, m^2
K = number of pixels in specific calculated region
r = radial coordinate, mm
d_s = particle diameter, mm
e = coefficient of restitution
Δt = time step, s
h = settled bed height, m
x = x position in the Wurster fluidized bed, cm
y = y position in the Wurster fluidized bed, cm
z = z position in the Wurster fluidized bed, cm

Greek letters

λ = normalized capacitance vector
α = step length or gain factor
τ = relaxation factor
β = average particle concentration
ϑ = packed bed concentration of experimental material, %
ρ_s = particle density, kg/m^3

Literature Cited

1. Wurster DE. Air-suspension technique of coating drug particles—a preliminary report. *J Am Pharm Assoc*. 1959;48:451–454.
2. Walker GM, Bell SEJ, Green K, Jones DS, Andrews GP. Characterisation of fluidized bed granulation processes using in-situ Raman spectroscopy. *Chem Eng Sci*. 2009;64:91–98.
3. Geldart D. Types of gas fluidization. *Powder Technol*. 1973;7:285–292.
4. Gidaspow D, Bezburuah R, Ding J. Hydrodynamics of circulating fluidized bed, Kinetic theory approach. In: Fluidization VII. Proc of 7th Eng. Foundation Conference on Fluidization, May 3–8, Brisbane, Australia, 1992:75–82.
5. Naelapaa K, Veski P, Pedersen JG, Anov D, JØrgensen P, Kristensen HG, Bertelsen P. Acoustic monitoring of a fluidized bed coating process. *Int J Pharm*. 2007;332:90–97.
6. Werner SR, Jones JR, Paterson AH, Archer RH, Pearce DL. Air-suspension particle coating in the food industry: part I—state of the art. *Powder Technol*. 2007;171:25–33.

7. Behzadi SS, Toegel S, Viernstein H. Innovations in coating technology. *Recent Pat Drug Deliv Formul*. 2008;2:209–230.
8. He YL, Lim CJ, Grace JR, Zhu JS, Qin SZ. Measurements of voidage profiles in spouted beds. *Can J Chem Eng*. 1994;72:229–234.
9. Saadevandi BA, Turton R. Particle velocity and voidage profiles in a draft tube equiipped spouted-fluidized bed coating device. *Chem Eng Commun*. 2004;191:1379–1400.
10. Karlsson S, Niklasson BI, Folestad S, Rasmuson A. Measurement of the particle movement in the fountain region of a Wurster type bed. *Powder Technol*. 2006;165:22–29.
11. Luštrik M, Šibanc R, Srčič S, Perpar P, Žun I, Dreu R. Characteristics of pellet flow in a Wurster coater draft tube utilizing piezoelectric probe. *Powder Technol*. 2013;235:640–651.
12. Du B, Warsito W, Fan LS. ECT studies of gas-solid fluidized beds of difference diameters. *Ind Eng Chem Res*. 2005;44:5020–5030.
13. Makkawi YT, Wright PC. Electrical capacitance tomography for conventional fluidized bed measurements-remarks on the measuring technique. *Powder Technol*. 2004;148:42–157.
14. Takei M, Zhao T, Yamane K. Measurement of particle concentration in powder coating process using capacitance computed tomography and wavelet analysis. *Powder Technol*. 2009;193:93–100.
15. Depypere F, Pieters JG, Dewettinck K. PEPT visualisation of particle motion in a tapered fluidized bed coater. *J Food Eng*. 2009;93:324–336.
16. Wang HG, Yang WQ. Scale up of an electrical capacitance tomography sensor for imaging pharmaceutical fluidized beds and validation by computational fluid dynamics. *Meas Sci Technol*. 2011;22:104015.
17. Guardiola J, Rojo V, Ramos G. Influence of particle size, fluidization velocity and relative humidity on fluidized bed electrostatics. *J Electrostat*. 1996;37:1–20.
18. Wang HG, Yang WQ, Senior P, Raghavan RS, Duncan SR. Investigation of batch fluidized-bed drying by mathematical modeling, CFD simulation and ECT measurement. *AIChE J*. 2008;54:427–444.
19. Wang HG, Senior PR, Mann R, Yang WQ. Online measurement and control of solids moisture in fluidised bed dryers. *Chem Eng Sci*. 2009;64:2893–2902.
20. Wang HG, Yang WQ. Measurement of fluidised bed dryer by different frequency and different normalisation methods with electrical capacitance tomography. *Powder Technol*. 2010;199:60–69.
21. Yang WQ, Spink DM, York TA, McCann H. An image reconstruction algorithm based on Landweber's iteration method for electrical capacitance tomography. *Meas Sci Technol*. 1999;10:1065–1069.
22. Ye JM, Yang WQ. Evaluation of electrical capacitance tomography sensors for concentric annulus. *IEEE Sens J*. 2013;13:446–456.
23. Ge RH, Ye JM, Wang HG. Comparison of electrical capacitance tomography sensors with internal-external electrodes. In: Proceedings of 2013 IEEE International Conference on Imaging Systems and Techniques, October 22–23, 2013, Beijing, China. 2013:31–34.
24. Perpar M, Luštrik M, Dreu R, Srčič S, Žun I. Estimating coating quality parameters on the basis of pressure drop measurements in a Wurster draft tube. *Powder Technol*. 2013;246:41–50.
25. Wang LK, Heng PW, Liew CV. Classification of annular bed flow patterns and investigation on their influence on the bottom spray fluid bed coating process. *Pharm Res*. 2010;27:756–766.
26. Wang SY, Hao ZHJ, Sun D, Wei LX, Wang S. Hydrodynamic simulations of gas-solid spouted bed with a draft tube. *Chem Eng Sci*. 2010;65:1322–1333.
27. Sudsakorn K, Turton R. Nonuniformity of particle coating on a size distribution of particles in a fluidized bed coater. *Powder Technol*. 2000;110:37–43.
28. Cheng XX, Turton R. The prediction of variability occurring in fluidized bed coating equipment. II: the role of nonuniform particle coverage as particle pass through the spray zone. *Pharm Dev Technol*. 2000;5:323–332.
29. Shelukar S, Ho J, Zega J, Roland E, Yeh N, Quiram D, Nole A, Katdare A, Reynolds S. Identification and characterization of factors controlling tablet coating uniformity in a Wurster coating process. *Powder Technol*. 2000;110:29–36.
30. Dawoodbhai S, Rhodes CT. The effect of moisture on powder flow and on compaction and physical stability of tablets. *Drug Dev Ind Pharm*. 1989;15:1577–1600.
31. Ding J, Gidaspow D. A bubbling fluidization model using kinetic theory of granular flow. *AIChE J*. 1990;36:523–538.
32. Wang HG, Yang WQ, Dyakowski T, Liu S. Study of bubbling and slugging fluidized beds by simulation and ECT. *AIChE J*. 2006;52:3078–3087.

Manuscript received May 23, 2014, and revision received July 25, 2014.